Applied Catalysis B: Environmental 166–167 (2015) 45–55

Contents lists available at ScienceDirect

Applied Catalysis B: Environmental

journal homepage: www.elsevier.com/locate/apcatb

Titanium dioxide/zeolite integrated photocatalytic adsorbents for the degradation of amoxicillin

Devagi Kanakaraju[a,1], Jutta Kockler[b], Cherie A. Motti[c], Beverley D. Glass[b], Michael Oelgemöller[a,*]

[a] College of Science, Technology and Engineering, James Cook University, Townsville, Qld 4811, Australia
[b] College of Medicine and Dentistry, James Cook University, Townsville, Qld 4811, Australia
[c] Australian Institute of Marine Science (AIMS), Biomolecular Analysis Facility, Townsville, Qld 4810, Australia

ARTICLE INFO

Article history:
Received 10 May 2014
Received in revised form 4 September 2014
Accepted 1 November 2014
Available online 7 November 2014

Keywords:
Photocatalysis
Natural zeolite
Integrated photocatalytic adsorbent
Titanium dioxide
Amoxicillin
Hydrolysis

ABSTRACT

Integrated photocatalytic adsorbents (IPA) prepared from TiO_2 and natural zeolite were applied to amoxicillin (AMX) degradation. The acid-alkali pre-treated zeolite annealed at 300 °C under nitrogen resulted in the best degradation of AMX. The superior performance of this IPA material was explained using scanning electron microscopy (SEM), energy-dispersive spectroscopy (EDS) and X-ray diffraction (XRD). SEM analysis showed an uneven surface as a result of TiO_2 cluster deposition, which provides more active sites for adsorption and degradation. XRD results revealed that peaks from more photoactive anatase were more prominent in this IPA material. EDS analyses also confirmed the presence of high amounts of TiO_2. Despite their large TiO_2 loadings, comparison experiments with untreated zeolite suggested that the pores are still available for adsorption. The overall performance of the IPA material for the degradation of AMX was thus attributed to the adsorption capability of the zeolite carrier, the photocatalytic activity of TiO_2 coating and acid-catalyzed hydrolysis ('capture & destroy'). Degradation products resulting from TiO_2/zeolite IPA-induced hydrolysis were identified by liquid chromatography-mass spectrometry (LC-MS) prior to photocatalytic treatment. AMX and its thermal degradants were almost completely removed after 240 min of irradiation. The efficiency of the developed TiO_2/zeolite material provides a potentially economical way of degrading pharmaceutical compounds and recovering photocatalysts simultaneously.

1. Introduction

Titanium dioxide (TiO_2) has been intensively studied as a heterogeneous photocatalyst and has demonstrated its potential for the degradation of organic compounds in aqueous systems [1,2]. A major difficulty encountered with this material is the time-consuming and uneconomical recovery of TiO_2 and the necessity for high photocatalyst loadings [3]. These drawbacks have limited the widespread technical application of heterogeneous photocatalysis in water treatment. To achieve pre-concentration of pollutants and improve the separation of TiO_2 particles, immobilization of TiO_2 on an adsorbent or an inert support to create integrated photocatalytic adsorbents (IPAs) has been proposed [4,5]. Using IPAs, degradation of pollutants can be achieved by the simultaneous effects of physical adsorption by the adsorbent and photochemical degradation by the immobilized TiO_2 ('capture & destroy'). To achieve this TiO_2 particles are typically dispersed on inert and high surface area supports such as activated carbon [5,6], zeolite [7,8], organic polymers [9] or alginate [10]. Of these materials, natural zeolites are especially promising for IPA syntheses as they are abundant in nature and inexpensive. Zeolites are hydrated aluminosilicate minerals consisting of three-dimensional structures of SiO_4 and AlO_4 tetrahedrally linked by oxygen atoms to form a cage-structure [11]. They are characterized by good adsorption abilities, uniform channels and regular pores [12]. The exact composition and consequently the physicochemical properties of natural zeolites vary with geographic location. Pre-treatment is thus commonly applied to enhance their adsorption efficiency. Ion exchange with inorganic salts and alkali bases as well as acid treatment and calcination at high temperature has been utilized to modify the surface structure of zeolite particles [13]. Due to their acidic nature,

* Corresponding author. Tel.: +61 7 4781 4543.
E-mail address: michael.oelgemoeller@jcu.edu.au (M. Oelgemöller).
[1] Present address: Department of Chemistry, Faculty of Resource Science and Technology, Universiti Malaysia Sarawak, 94300, Kota Samarahan, Sarawak, Malaysia.

http://dx.doi.org/10.1016/j.apcatb.2014.11.001
0926-3373/

zeolites are frequently used as solid acid catalysts [14]. This feature makes them interesting materials for the photodegradation of pollutants by targeted pH-alteration [15]. Likewise, TiO_2 can be readily supported in the existing cage-structure or channels of the zeolite particles. Studies of TiO_2/natural zeolite IPAs mostly report on organic compounds such as dyes [16–18] and humic acids [7]. In contrast, these materials have not been studied for the degradation of pharmaceutical compounds, which have recently emerged as significant environmental pollutants [19–21].

Amoxicillin (AMX) [22], a β-lactam antibiotic, was selected for the current study as it is a widely human and veterinary medicine [23]. Due to its slow rate of metabolism in humans, oral administration of 500 mg of AMX in humans has resulted in the excretion of 86 ± 8% in the urine within two hours of consumption [24]. Although sensitive towards hydrolysis under a variety of pH conditions [25,26], AMX is difficult to degrade completely and it can be found in both urine and faeces, along with its hydrolysed and metabolised by-products [27]. In Australia, AMX has emerged as one of the most frequently prescribed medicines and has been reported to be present used in river water and hospital effluents in ng/L levels [28]. Only partial removal of antibiotics is generally achieved by conventional urban wastewater treatment plants (WWTPs), making this class of drugs important pollutants [29]. The widespread usage of AMX and its frequent detection in the environment highlights the need for its removal.

Most advanced oxidation processes for the degradation of AMX in water matrices have focused on Fenton/photo-Fenton [30–36], ozonation [37,38] or UV/H_2O_2 [39]. Photocatalysis studies have reported the use of TiO_2 [24,33,40–44] or ZnO [45] for the removal of AMX. A study by Klauson et al. utilized doped and undoped titania [44], while a TiO_2/activated carbon (AC) derived IPA was investigated by Basha and co-workers [6] for its degradation. In the latter study, results showed that 10% TiO_2/AC produced the highest removal of 87% for a 150 mg/L AMX solution after 150 min of irradiation.

In this study, TiO_2/natural zeolite IPAs were prepared, characterized and subsequently evaluated for the degradation of AMX in water. The extent of mineralization was furthermore determined by measuring dissolved organic carbon (DOC). For the most efficient IPA material prepared, degradation by hydrolysis (during initial adsorption) and photocatalysis under several conditions was monitored by liquid chromatography-mass spectrometry (LC-MS).

2. Experimental

2.1. Materials and methods

Titanium (IV) isopropoxide ($C_{12}H_{28}O_4Ti$, TTiP, 95%, Alfa Aesar), absolute ethanol (AR grade, Univar, Australia), nitric acid (AR, BDH Chemical), hydrochloric acid (AR grade, Ajax Finechem Pty Ltd, Australia), sodium hydroxide (AR grade, Ajax Finechem Pty Ltd) and amoxicillin (R&D grade, Sigma–Aldrich) were used as received. Titanium dioxide P25 Aeroxide® (80% anatase and 20% rutile, BET surface area 50 m^2/g) was supplied by Evonik industries. Natural Australian zeolite (Escott zeolite regular powder, <75 μm) was obtained from Zeolite Australia Pty Limited (NSW, Australia). For the pH determination study, reverse osmosis water was prepared with a Millipore® Elix 10 from Millipore SAS. For all other applications, Milli-Q water from a Barnstead Nanopure Diamond water ion exchange system (18.2 MΩcm resistivity) was used.

2.2. Preparation of integrated photocatalytic adsorbent

The raw Escott zeolite used in this study consisted of the zeolitic mineral clinoptilolite, with traces of mordenite, quartz, clay and mica. The zeolite supplied was analysed for its composition by energy dispersive X-ray spectroscopy (EDS), which revealed SiO_2 (72.3%) and Al_2O_3 (11.6%) as the major constituents.

2.2.1. Pre-treatment of natural zeolite

Zeolite (20 g/L) was vigorously stirred in deionized water for 5 h and the resulting suspension was allowed to settle prior to filtration and further washing with deionized water. Two types of treatments were performed on this zeolite sample: (i) an acid activation and (ii) a combination of acid-alkali activation. For the acid activation, the zeolite was treated with 1 M HCl for 24 h with continuous stirring. For the acid-alkali activation, the initial treatment was performed with 1 M HCl and was followed by 1 M NaOH. Contact times of zeolite with each reagent were kept to 5 h and vigorous stirring was applied. The pre-treated zeolite was continuously washed with deionized water and dried in a laboratory oven at 70 °C for 24 h, followed by heat treatment at 300 °C in a furnace oven (LABEC Model HTFS 60/13).

2.2.2. Synthesis of TiO_2/zeolite

TiO_2/zeolite IPAs were synthesized following a modified procedure by Huang and co-workers [12]. TTiP (0.1 mol) was dissolved slowly in 100 mL of absolute ethanol. A white sol formed within 10 min. Concentrated HNO_3 was added dropwise until the white precipitate disappeared and a transparent sol formed. The final pH of the transparent sol was adjusted to a pH value of 4 and stirred continuously for 6 h at room temperature to give a transparent yellow sol. The zeolite was added into the sol at a mass ratio of 1:5 (zeolite:TiO_2) and stirred until a gel was formed. The TiO_2/zeolite was aged at room temperature for 24 h. Subsequently, it was oven-dried at 70 °C for 10 h and ground in a mortar to obtain a homogeneous material. These steps were performed for both acid activated and acid-alkali activated zeolites. The prepared TiO_2/zeolite samples were calcined at 300 °C and 450 °C in a nitrogen flow in a horizontal split tube furnace (LABEC Model HTFS 60/13) for 2 h. For comparison, pure TiO_2 was also prepared, using the same procedure, but without the addition of pre-treated zeolite.

2.3. Characterization of TiO_2/zeolite

Scanning electron microscopy (SEM) images of the TiO_2/zeolite materials were recorded using a JEOL scanning electron microscope (JSM-5410LV) at an accelerating voltage of 10 kV. The X-ray diffraction (XRD) patterns of the prepared materials were recorded on an X-ray diffractometer (Siemens D5000) using Ni filtered Cu Kα radiation (λ = 1.5406) from 2θ = 2–65°. EDS (JEOL JXA-8200) was used to characterize the synthesized IPAs and zeolite materials for their compositions.

2.4. Dark adsorption studies

AMX solutions of various concentrations (5, 10, 30 and 50 mg/L) were prepared and 100 mL of each solution was transferred into a 150 mL conical flask. IPA materials prepared by acid-alkaline treatment and calcined at 300 °C (0.1 g) were added and the suspensions were agitated with exclusion of light for 24 h on an orbital shaker (Stuart Model SSL1). Aliquots were collected and filtered through a 0.22 μm syringe filter prior to high-performance liquid chromatography (HPLC) analysis.

2.5. pH studies

An AMX stock solution (30 mg/L) was freshly prepared and 20 mL portions were transferred into 50 mL polypropylene centrifuge tubes. Zeolite, TiO_2 or IPA materials (40 mg) were added and the suspensions were agitated with exclusion of light for a

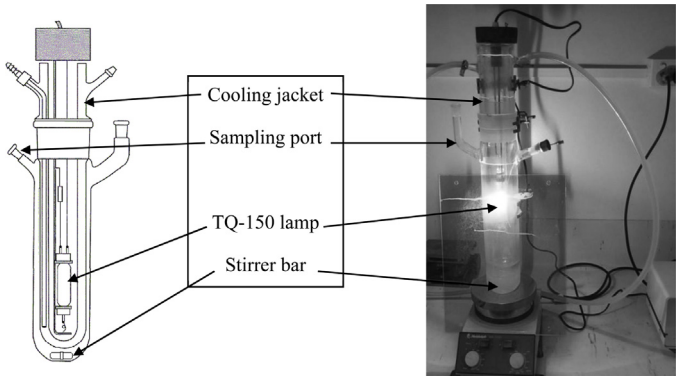

Fig. 1. Schematic representation and photograph of the immersion-well photoreactor setup.

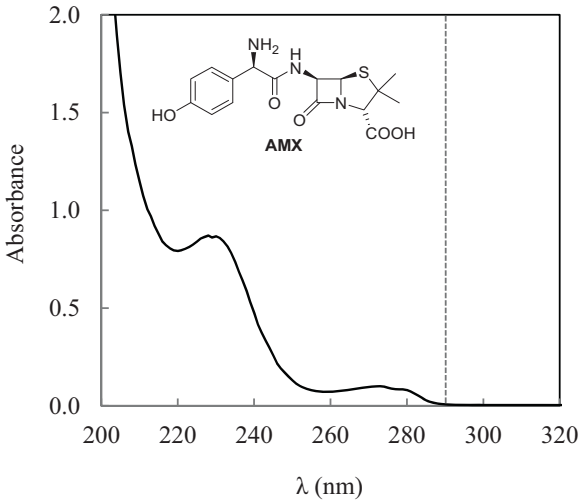

Fig. 2. Absorbance spectrum of AMX (inset) in water. The cut-off wavelength of Pyrex glass of the immersion-well photoreactor is shown as a vertical line.

total of 24 h on a flask shaker (Stuart Model SF1). pH values were determined initially and after 30 min, 1, 4.5 and 24 h with a pH-meter (labChem-CP) equipped with an intermediate junction pH electrode (Model IJ44C). Experiments were conducted in duplicate.

2.6. Photocatalytic degradation experiments

The photocatalytic degradation experiments involving AMX were carried out using an immersion-well reactor (optical path: ~0.5 cm) and 250 mL of an aqueous medium (Fig. 1). A medium pressure Hg-lamp (TQ-150, Peschl Ultraviolet GmbH, average radiation flux between 200 and 600 nm: 47 W) was placed in the centre of the Pyrex cooling jacket (cut-off wavelength ≤290 nm) and a magnetic stirrer used to provide a homogeneous dispersion. Slow stirring at 700 rpm was maintained to minimize mechanical damage to the IPA, however, IPA material constantly settled on the bottom of the reactor vessel during operation. Chilled water was used for cooling, which ensured that the internal temperature within the reactor remained below 29 °C. The concentration of AMX for the degradation experiments was fixed at 30 mg/L. With the exception of the catalyst concentration study, a loading of 2 g/L was generally used for TiO_2/zeolite and pure TiO_2.

Prior to irradiation, the reaction mixture was stirred continuously for 30 min to allow for adsorption of AMX onto the surface of the IPA. Experiments were performed at inherent solution pHs, which were uncontrolled during irradiations. Samples were withdrawn at set times after the dark adsorption period and during irradiation, centrifuged at 1,000 rpm for 15 min (Mini Spin Plus, Eppendorf) and filtered through a 0.22 μm syringe filter to remove any suspended particles from the solution. This was followed by HPLC (LC-940 Varian) analyses monitored at the main absorption maximum (λ_{max}) of AMX in water at 230 nm (Fig. 2). Samples withdrawn were analysed immediately. Experiments were run in duplicate and mean values were used. The standard deviation did not exceed 5%, thus showing good reproducibility.

For the recycling study, the TiO_2/zeolite material from each previous photocatalysis study was filtered, washed with deionized water and dried at 70 °C for 1 h. The material was tested for its photocatalytic degradation capability in subsequent reaction cycles using fresh solutions of 30 mg/L of AMX. No more than three cycles were investigated due to the incomplete recovery of IPA (material recovery of approximately 90% per cycle). A direct photolysis experiment in the absence of any photocatalyst was also performed. To measure the degree of mineralization during direct photolysis and selected photocatalysis runs, DOC analyses were performed using filtered samples (0.45 μm GF/F filter) on a Shimadzu TOC analyser (Model 5000A) equipped with an ASI-5000A autosampler. All organic (and inorganic) matter larger than 0.45 μm is filtered off, whereas AMX and its potential degradation products (incl. its higher oligomers) remain in the samples.

2.7. Analyses

AMX concentrations were determined by HPLC using an Agilent 1100 system equipped with a degasser, an auto-injector, a binary pump and a PDA detector. Chromatographic separation was achieved isocratically with KH_2PO_4 (pH 4)/MeOH, 90/10 (v/v) using a reverse-phase Phenomenex XB-C18 150 × 4.6 mm (2.6 μm) column at 25 °C and a flow rate of 0.5 mL/min. The injection volume was 20 μL and AMX was monitored at λ = 230 nm. All analyses were carried out in duplicate to confirm reproducibility.

For further degradation monitoring, LC-MS was used but required a different mobile phase due to possible interference of the potassium buffer during electrospray ionisation (ESI). For LC-MS, the HPLC instrument was operated in gradient mode using the same flow rate, injection volume and column as described above. The mobile phase consisted of 0.1% formic acid in water (mobile phase A) and 0.1% formic acid in acetonitrile (mobile phase B). The gradient elution was as follows: 5 min 95% A/5% B, 15 min 100% B and then a return to the initial conditions for 5 min. The HPLC was connected to a Bruker Esquire 3000 ion trap mass spectrometer with an Apollo ESI ion source operating in ESI positive mode. All LC-MS data were collected using Bruker Daltonics Esquire Control v5.3 and Hystar v3.1 operating on Windows XP Professional. The operating conditions were as follows: nebulizer gas: 20 psi; drying gas: 6.0 mL/min; drying temperature: 350 °C. MS spectra were acquired over an m/z range of 50–2000. The presence of the parent and product ions was determined by monitoring the base peak chromatogram (BPC) and the extracted ion chromatograms (EIC).

3. Results and discussion

3.1. IPA characterization

The SEM images of natural zeolite showed a relatively smooth surface (Fig. 3a). Both acid (Fig. 3b) and acid-alkali (Fig. 3c) treatments significantly altered the surface structure with the acid-alkali treated zeolites, demonstrating greater surface irregularity. SEM images of both TiO_2/zeolites showed rough, jagged and uneven surfaces as a result of TiO_2 being deposited in clusters of irregular shapes, exemplified by the IPAs calcined at 300 °C in Fig. 3d and e.

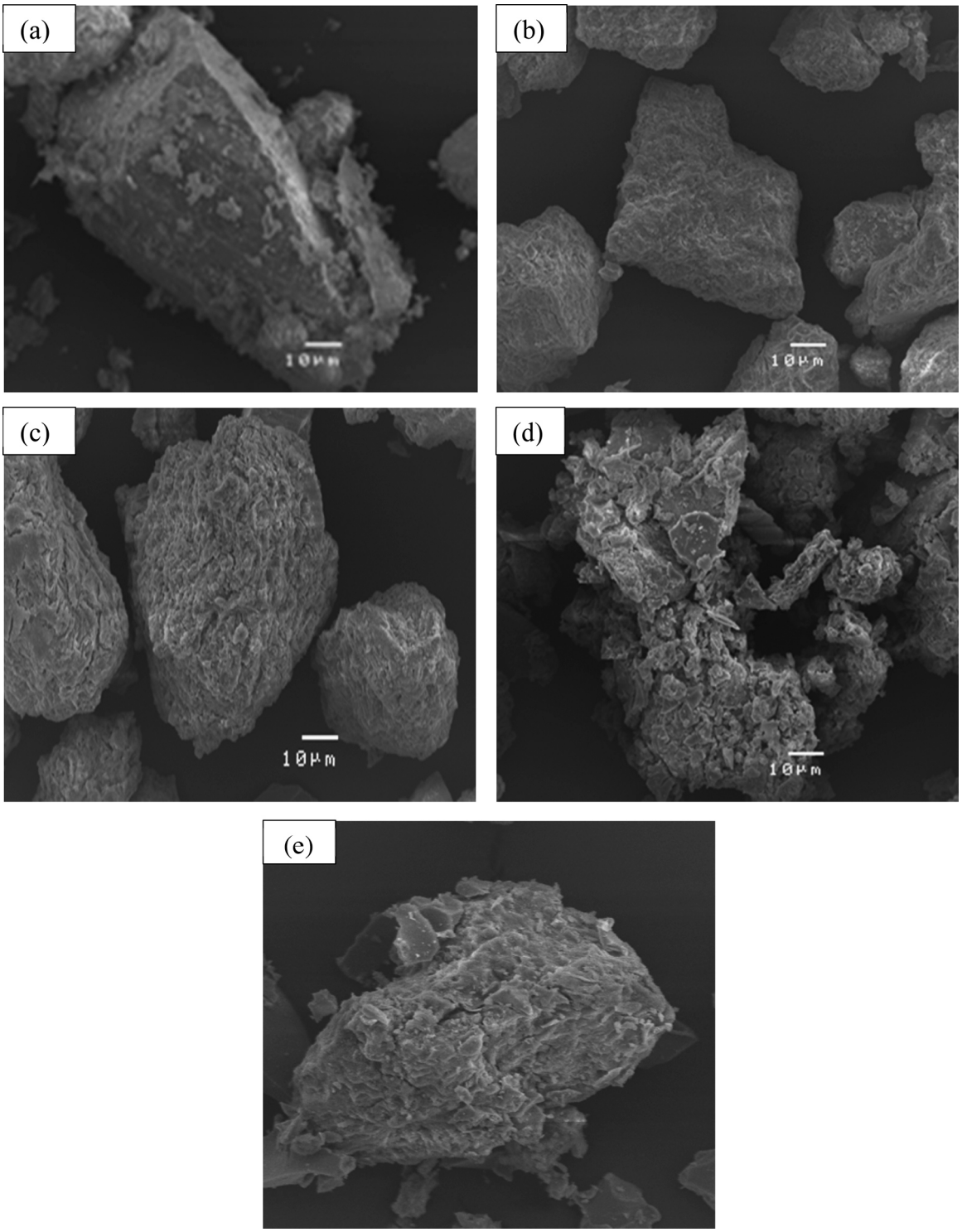

Fig. 3. SEM images of the materials: (a) natural zeolite, (b) acid-treated zeolite, (c) acid-alkali treated zeolite, (d) TiO_2/zeolite acid-alkali (300 °C) and (e) TiO_2/zeolite acid (300 °C).

EDS analyses conducted with the TiO_2/zeolite materials calcined at 300 °C revealed the presence of a higher TiO_2 content with approximately 74% in the acid-alkali treated TiO_2/zeolite compared to 52% for the acid-treated TiO_2/zeolite (Table 1). The higher proportion of TiO_2 correlated with lower levels of SiO_2 and Al_2O_3 in the samples, indicating that the acid-alkali treatment is more efficient in removing these Si and Al oxides than acid treatment alone. In the current case, a combination of pre-treatments has simultaneously increased the surface roughness and the TiO_2 content [46]. The IPA

Table 1
Quantitative analysis of IPA with EDS.

IPA	Metal oxide (%)		
	TiO_2	SiO_2	Al_2O_3
TiO_2/zeolite acid-alkali (300 °C)	74.2	23.3	2.5
TiO_2/zeolite acid (300 °C)	52.5	43.5	4.0

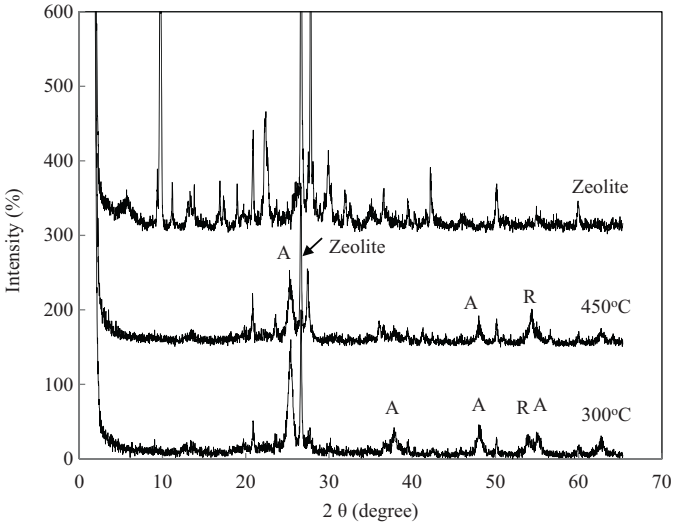

Fig. 4. XRD pattern of zeolite and TiO_2/zeolites from acid-alkaline pre-treatment calcined at 300 °C and 450 °C (A = anatase and R = rutile).

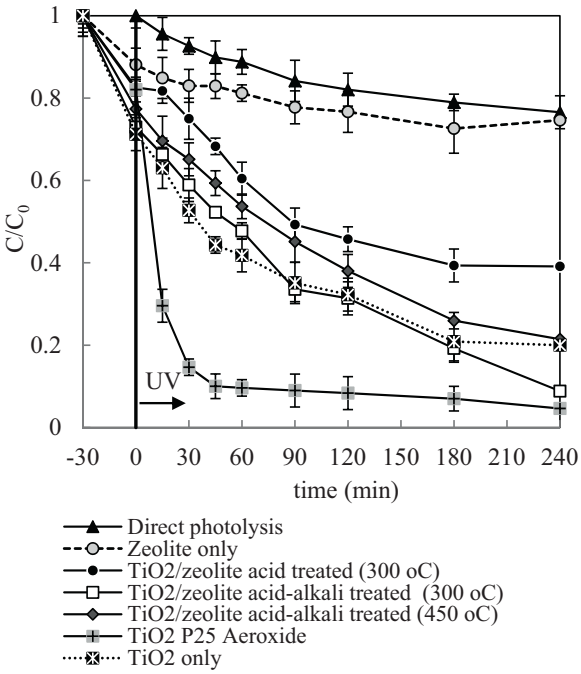

Fig. 5. Degradation of AMX under different conditions (C_0 = 30 mg/L; catalyst concentration: 2 g/L).

obtained from acid-alkaline treatment was thus chosen for further studies.

The crystal phase of the prepared IPA materials from acid-alkaline pre-treatment was studied by XRD. The XRD patterns of the TiO_2/zeolite samples were subsequently compared to that of natural Escott zeolite (Fig. 4), which was found largely identical to that of pure clinoptilolite [47]. After treatment, the main peak for the most stable rutile polymorph of TiO_2 is typically found at $2\theta = 27.7°$. However, the natural zeolite also displays a signal at $2\theta = 27.7°$ and therefore this characteristic peak could not be used to confirm the presence of the TiO_2 rutile polymorph. Despite this limitation, the XRD results revealed a mixed phase of TiO_2 anatase and rutile polymorphs.

Anatase peaks were prominent in the IPA samples calcined at 300 °C, however, when the temperature was increased to 450 °C, the intensity of the characteristic anatase peaks corresponding to $2\theta = 25.4°$ decreased, while the rutile peak at $2\theta = 54.3°$ became stronger and sharper. The main peak of the zeolite (at $2\theta = 27.7°$) remained unchanged regardless of the temperature, suggesting that the frame structure of zeolite remained intact after TiO_2-loading [48]. Compared to the XRD pattern of pure zeolite, the intensities of some diffraction peaks of the IPA material decreased or disappeared, which was due to coverage of the zeolite surface by TiO_2. Similar observations have been reported by Huang et al. [12]. Anatase was determined to be the predominant phase, which is advantageous due to its higher photocatalytic activity [49,50]. Higher calcination temperatures between 550 and 800 °C have been reported to initiate the conversion of anatase to rutile, with factors such as the preparation conditions and the chemical treatments also influencing this process [51]. As demonstrated by Zhu and co-workers, TiO_2/zeolite calcined at 200 °C was found to consist of anatase, rutile and trace amounts of brookite polymorphs, whereas calcination at intermediate temperatures of 300 °C and 450 °C produced only a mixture of the anatase and rutile polymorphs [52].

The high loading and surface irregularities of the IPAs suggest that the deposition of TiO_2 predominately occurred on the zeolite surface and not within its pores. Although Brunauer-Emmett-Teller (BET) measurements could not be carried out, related studies reported a decrease in BET surface area due to TiO_2 immobilization [7,53–56]. Similar effects are thus proposed for the present IPA materials.

3.2. Photolytic and photocatalytic degradation of amoxicillin

Due to its favourable characteristics, most experiments were conducted using TiO_2/zeolite IPAs obtained from acid-alkali treatment and calcination at 300 °C. Limited experiments were conducted with other IPA materials for comparative purposes.

3.2.1. Dark adsorption

Adsorption is known to be an integral part of heterogeneous photocatalysis [2]. In general, TiO_2 particles show a strong affinity for highly polar or ionisable groups [57], which are both present in AMX. Using the TiO_2/zeolite material from acid-alkali treatment and calcined at 300 °C, the percentage removal for 5, 10, 30 and 50 mg/L solutions of AMX after 24 h was found to be 9, 10, 14 and 9%, respectively. This shows that although adsorption alone contributes only marginally to the elimination process of AMX, partial acid-catalysed hydrolysis cannot be ruled out. The drop in removal efficiency for the highest IPA loading may have alternatively been caused by aggregation of the particles.

3.2.2. Photodegradation studies

The photodegradation of AMX investigated under the different conditions are presented in Fig. 5. Although previous studies have demonstrated the photostability of AMX towards direct photolysis with visible light [41,42], some degradation occurred during this study with a 23% reduction in AMX after 240 min of irradiation with light emitted from a UV-lamp. This low photolytic decomposition is attributed to the poor absorption of AMX above 290 nm, the cut-off wavelength of the chosen of the Pyrex glass of the immersion-well photoreactor (Fig. 1). Hence the results confirm that direct photolysis contributed only marginally to the degradation of AMX. As would be expected, higher degradation rates were reported with UV-C light or in the presence of H_2O_2 [39].

Exposure of AMX to TiO_2-free, untreated natural zeolite revealed a removal of only 15% after 240 min of irradiation. The degree of elimination was thus in the same range as those for direct photolysis or (dark) adsorption. The latter finding suggests that the pores of the IPA zeolite material have not been completely blocked

and that they are still available for adsorption. A similar study by Li et al. also showed that the natural zeolite modernite did not participate in the photolytic (365 nm) degradation of the dye Orange II [58].

Photocatalytic degradations of AMX were likewise performed with three TiO_2/zeolite IPA materials prepared using different pre-treatments and calcination temperatures (Fig. 5). In comparison to direct photolysis and degradation in the dark, elimination rates increased but a clear dependence on pre-treatment as well as calcination temperature was observed. Calcination temperatures below 200 °C were not considered for the preparation of TiO_2/zeolite because they are known to produce a poor TiO_2 crystallinity, which consequently affects its photocatalytic activity in the degradation process [59]. The TiO_2/zeolite obtained from acid treatment and calcined at 300 °C resulted in a removal of 61% after 4 h of irradiation. Both materials produced from acid-alkali treatment showed even higher degradation efficiencies. Of these, the material from calcination at 300 °C was found to yield the greatest degradation of 88%, compared to that prepared at 450 °C with 72%. The former material was therefore chosen for all subsequent experiments. The superior performance of the TiO_2/zeolite material calcined at 300 °C correlated with SEM and EDS results. The surface of the acid-alkali treated zeolites showed the highest degree of irregularities, thus offering more active sites for adsorption and photocatalytic degradation. EDS analyses furthermore revealed the highest TiO_2 and thus photoactive catalyst content. Whereas elevated calcination temperature enhances the formation of the more photoactive TiO_2 anatase phase, conglomeration of catalyst particles reduces the specific surface area and consequently the photocatalytic performance. A similar finding has been reported by Shi et al. [60] for the removal of phenol. Calcination at lower temperature was also found to be beneficial for Pt-modified TiO_2 on natural zeolite [12]. The superior performance of TiO_2/zeolite obtained from acid-alkali treatment and calcined at 300 °C in this study is primarily a result of the enhanced surface roughness.

In order to compare the photocatalytic activity of the synthesized TiO_2/zeolite materials, pure synthesized TiO_2 was also examined. While the same loadings of 2 g/L of materials were used, the hybrid TiO_2/zeolite materials naturally displayed a much lower TiO_2 content compared to that of the pure photocatalyst. Despite this, TiO_2/zeolite from acid-alkali treatment and calcined at 300 °C demonstrated a greater overall ability to remove AMX upon prolonged irradiation (Fig. 5), although synthesized TiO_2 performed better during the first 60 min. After 4 h of irradiation, the percentage AMX degradation obtained with pure TiO_2 was 79%, while the TiO_2/zeolite material increased the degradation to 88%. This finding confirms that the photocatalytic activity of TiO_2 did not decline once anchored to zeolite. The same phenomenon was also observed when TiO_2/fly ash was compared with TiO_2 alone for phenol degradation [60]. The higher degradation rate obtained for the TiO_2 supported on zeolite can be attributed to its higher adsorption capacity, similar to that reported by Sharma and co-workers for the degradation of the herbicide isoproturon over a TiO_2/H-MOR composite [61]. This finding thus once again confirms the exposure of the zeolite pores, at least in part, in the IPA material. The degradation of AMX with the highly photoactive TiO_2 P25 was found to be more efficient than with the IPAs prepared with approximately 95% degrading after 4 h. TiO_2 P25 is regarded as one of the best photocatalysts and is thus commonly studied as a reference material [62]. While TiO_2 P25 was used in its pure form, the actual amount of TiO_2 for the hybrid IPA material was naturally lower, which may somewhat explain its poorer performance. In addition, the zeolite carrier material scatters light, thus reducing its penetration into the reaction mixture. An advantage of the synthesized IPA over TiO_2 P25 is its simple recovery from the solution by filtration after irradiation, which is not easily achieved for the finer TiO_2 P25 particles.

Table 2
pH determination studies using a standard AMX solution (30 mg/L).

Additive	pH (mean)				
	0 min	30 min	1 h	4.5 h	24 h
None	5.47	5.55	5.45	5.14	5.04
TiO_2 P25	4.05	4.12	4.11	3.93	4.04
Zeolite (untreated)	6.29	6.23	6.24	6.07	5.98
Synthesized TiO_2	2.97	2.90	2.87	2.75	2.74
TiO_2/zeolite acid (300 °C)	5.34	5.36	5.32	5.39	5.25
TiO_2/zeolite acid-alkali (300 °C)	2.99	3.00	3.01	2.95	2.91

Additionally, the adsorption capacity of TiO_2/zeolite was considerably higher than that of TiO_2 P25 and its acidic nature may have assisted degradation by partial hydrolysis.

3.2.3. pH determinations

The pH of the reaction medium has a significant effect on both the photocatalyst TiO_2 and the substrate AMX. For TiO_2 P25, the zero point charge (pH_{zpc}) has been reported to be 6.25 [1]. The zero point charge of the TiO_2/zeolite IPA obtained from acid-alkali treatment and calcination at 300 °C was determined to be 5.52 [27], confirming the acidic nature of the zeolite carrier [14]. Consequently, the surfaces of the photocatalysts are positively charged at $pH < pH_{zpc}$ and negatively charged at $pH > pH_{zpc}$. AMX displays different ionization stages owing to its various ionisable functional groups, carboxyl ($pK_{a1} = 2.68$), amine ($pK_{a2} = 7.49$) and phenol ($pK_{a3} = 8.94$) [38]. Zia et al. reported that AMX was stable towards hydrolysis within a pH range of 5.5–6.5 [25]. Trovó and co-workers did not observe any degradation of AMX after 5.5 h at its natural pH of 6.2, however, 74% of AMX was hydrolysed at pH 2.5 after the same time period [32]. Gozlan et al. examined the stability of AMX in phosphate buffer solutions at pH 5, 7 and 8 over time and determined the highest AMX stability at a pH of 5 [63]. Hydrolysis was faster under alkaline conditions. Likewise, metal ions were found to accelerate AMX hydrolysis. Similarly, Doadrio and Sotelo determined the rate of AMX hydrolysis over a pH range of 2–7 and determined the maximum stability at a pH of 5.51 [64].

Since hydrolysis may contribute significantly to the overall degradation of AMX under the chosen irradiation conditions, a pH study was conducted using a standard AMX solution (30 mg/L) and 2 g/L loadings of solid additive, e.g. zeolite, TiO_2 or IPA. After shaking in the dark, the pH values of the slurries were determined in intervals over a period of 24 h (Table 2). In the absence of any solid material, the natural pH of the AMX solution was found around 5.5 and decreased afterwards to 5.04. In the presence of untreated zeolite, the pH of the suspension initially increased to 6.29 and decreased to 5.98 after 24 h. The addition of TiO_2 P25 dropped the pH of the suspension to 4.05, which then remained effectively constant. When IPA prepared solely by acid treatment was added to the AMX solution, the pH decreased to 5.34 and finally to 5.25. In line with the findings by Zia et al. [25] and Gozlan and co-workers [63], thermal hydrolysis of AMX can thus be ruled out in all four cases. During the initial dark period, AMX removal was subsequently caused primarily by adsorption. In contrast, the pH of the reaction mixture decreased considerably to 2.97 and finally 2.74 when pure synthesized TiO_2 was present. Using the findings by Trovó and co-workers as a guide [32], hydrolysis was thus expected to contribute significantly to AMX removal in this pH range. A similar pH change was observed for the IPA material from acid-alkali treatment and calcined at 300 °C with pH values ranging from 2.99 to 2.91. Hence thermal degradation by hydrolysis clearly contributed to the overall removal of AMX for this material. With its surface largely positively charged in this pH range, adsorption between AMX and its thermal degradants is expected to be highly efficient. In all cases examined, AMX predominantly existed in its zwitterionic,

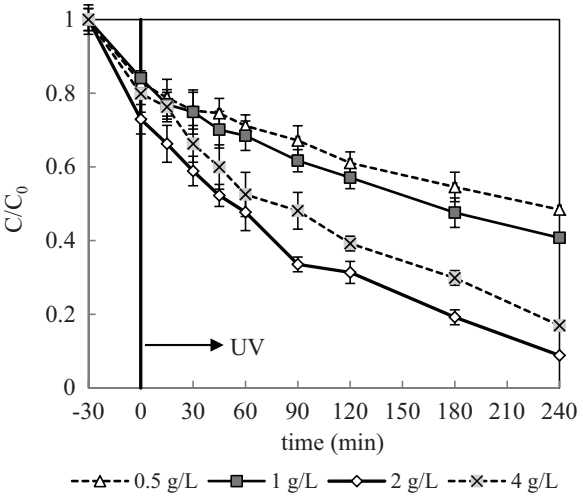

Fig. 6. Effect of catalyst concentration on the degradation of 30 mg/L AMX.

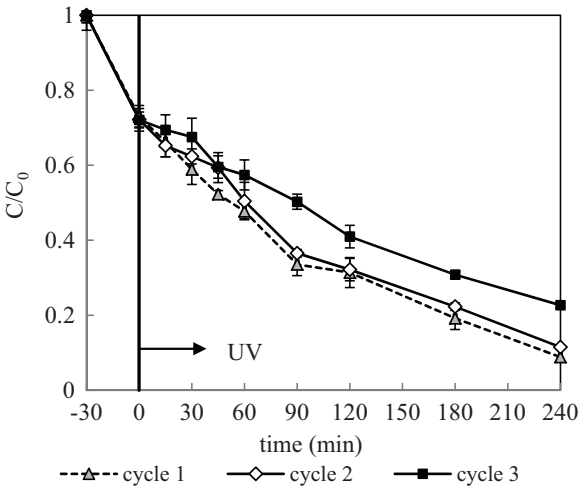

Fig. 7. Performance of recycled TiO_2/zeolite for AMX degradation.

neutral form [40], thus allowing for interactions with the photocatalysts and zeolite carrier.

3.2.4. Effect of catalyst concentration

To determine the optimum catalyst concentration, the degradation of AMX was performed with four loadings of the most active TiO_2/zeolite (acid-alkali treatment and calcined at 300 °C), 0.5 g/L, 1 g/L, 2 g/L and 4 g/L (Fig. 6). Degradation increased with the concentration of catalysts up to 2 g/L, but decreased when the concentration was further increased to 4 g/L. At high TiO_2-loadings, the degradation efficiency decreases due to light scattering phenomenon, which consequently causes reduction in light penetration into the reaction mixture [65]. The lower light transparency thus resulted in a reduction of $HO^{\bullet}$ radical formation [61]. In addition, adsorption during the dark period slightly increased for 2 g/L compared to the other catalyst loadings. As 2 g/L resulted in the highest removal, this concentration was considered optimal and used in all further experiments.

3.3. Catalyst recycling

A catalyst recycling study was conducted to determine the stability of the synthesized material over three cycles. While the dark adsorption/degradation efficiency was maintained, a decrease in the photocatalytic activity was observed upon repeated usage. Degradation of 88% was achieved during the first cycle, which decreased to 83% in the second cycle and eventually to 69% after the third use (Fig. 7). This loss of photocatalytic activity is possibly due to the accumulation of AMX and its degradation products on the surface and within the pores of the zeolite, blocking the available active sites for adsorption and consequently passivating the TiO_2 photocatalyst. Both phenomena gradually decreased the overall photocatalytic activity of the TiO_2/zeolite material. Likewise, only about 90% of the IPA could be recovered after each cycle, thus naturally reducing the amount of photocatalyst material available. A similar reduction in photocatalytic activity due to passivation has been reported by Gomez and co-workers for the degradation of the insecticide dichlorvos [53]. Photoactivity may have been restored by subsequent calcination as shown by Sharma and co-workers for TiO_2/mordenite hybrid materials [61]. However, this energy-intensive regeneration process was not adopted in this study.

3.4. Mineralization

The extent of mineralization was compared for four different experiments over the course of 240 min of irradiation (Fig. 8): direct photolysis, photocatalysis with TiO_2/zeolite from acid-alkali treatment and calcined at 300 °C, pure TiO_2 synthesized and TiO_2 P25. In line with the degradation results, only a negligible mineralization of 3% was achieved with direct photolysis. TiO_2/zeolite, despite inducing high levels of AMX degradation, was unable to achieve complete mineralization. Nonetheless, DOC was reduced by as much as 25% with this material clearly showing that photocatalytic decomposition had occurred. In contrast, hydrolysis alone does not result in any significant mineralization [32]. Synthesized TiO_2 alone also reduced the DOC by 23% and was thus in the same range as the TiO_2 supported on zeolite. Even the highly photoactive TiO_2 P25 resulted in an incomplete mineralization of just 36% after the same irradiation time. The intermediates formed during photocatalytic degradation likely caused the slow degree of mineralization observed as they compete for adsorption and subsequent photocatalytic degradation. Some of the degradants may also be more resistant to further oxidation as, for example, observed during photo-Fenton treatment of AMX [35].

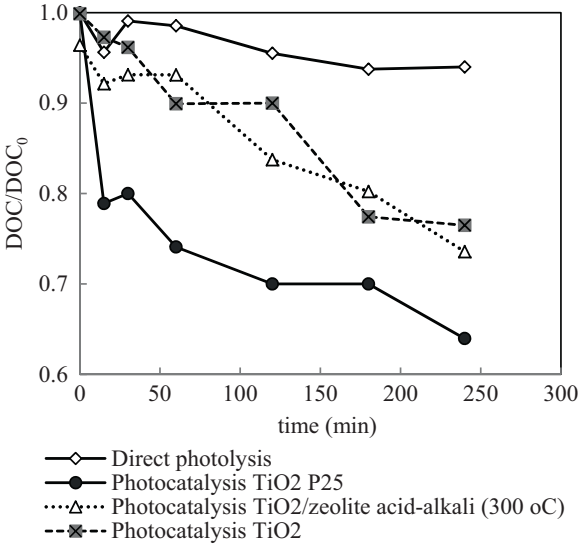

Fig. 8. DOC removal during direct photolysis and photocatalysis of AMX with TiO_2/zeolite and pure TiO_2.

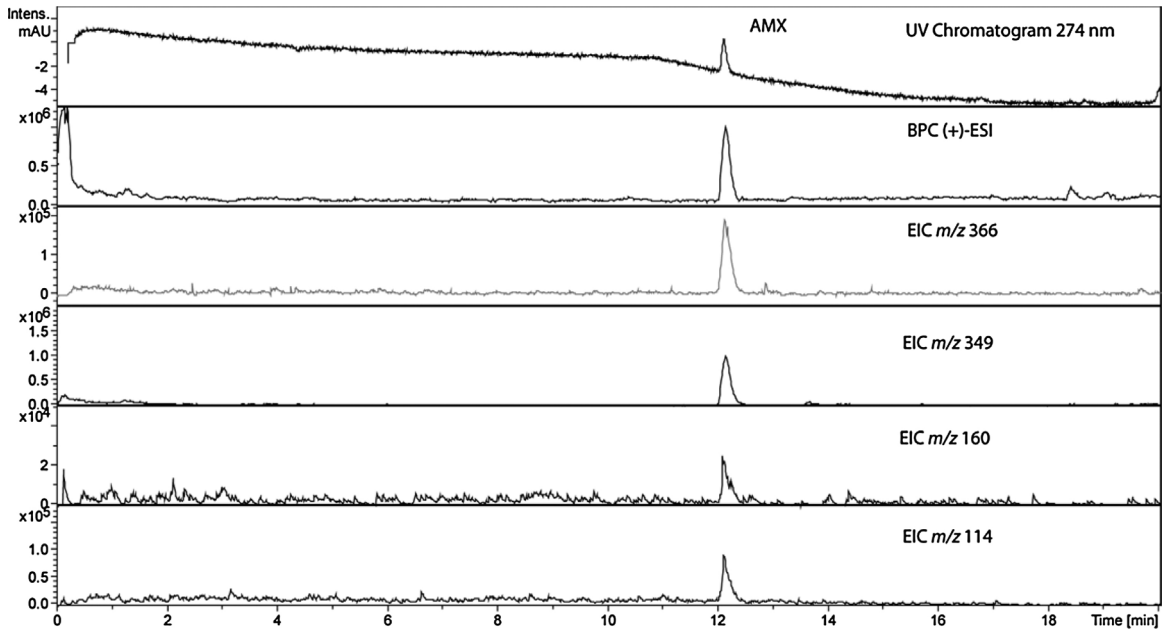

Fig. 9. LC-MS analysis of the AMX standard. The top spectrum shows the UV (274 nm) chromatogram, followed by the BPC. The subsequent EIC chromatograms show the specific ions formed.

3.5. LC-MS studies

LC-MS analysis of AMX ($M = C_{16}H_{19}N_3O_5S$; molecular weight = 365 g/mol; t_R = 12.2 min) resulted in the detection of the parent ion and three fragment ions (Fig. 9): *m/z* 366 $[M+H]^+$, 349 $[M+H\text{-}NH_3]^+$, 160 $[M+H\text{-}NH_3\text{-}CO\text{-}C_9H_7O_2N]^+$ and 114 $[M+H\text{-}NH_3\text{-}CO\text{-}C_9H_7O_2N\text{-}CO_2H_2]^+$. All of these ions have been described in earlier studies [32,66,67].

For the TiO_2/zeolite from acid-alkali treatment and calcination at 300 °C, thermal degradation of AMX was confirmed by LC-MS analyses. After several hours in the dark, AMX was almost completely degraded and numerous new peaks appeared in the LC-MS spectrum (Fig. 10a). Hydrolysis is known to yield a multitude of smaller break-down products as well as higher oligomers [26,32,63,68–70]. By comparison with literature spectra, three major degradation products resulting from hydrolysis could be identified (Fig. 11, Table 3). Initial opening of the β-lactam ring of AMX led to the formation of diasteroisomeric amoxicillin penicilloic acids (APcA), which were assigned based on their characteristic fragmentation peaks at *m/z* of 367. These compounds undergo further decarboxylation to generate a stereoisomeric mixture of amoxicillin penilloic acids (APlA) with typical ion

Table 3
Hydrolysis products of AMX detected by LC-MS in (+)-ESI mode.

t_R (min)	Formula	EIC (*m/z*)	Observed ion
8.5	$C_{16}H_{21}N_3O_6S$	384 [M + 1]	$[C_{16}H_{21}N_3O_6S+H]^+$
	(383 g/mol)	367	$[C_{16}H_{21}N_3O_6S+H\text{-}NH_3]^+$
	APcA[1]	349	$[C_{16}H_{21}N_3O_6S+H\text{-}NH_3\text{-}H_2O]^+$
		340	$[C_{16}H_{21}N_3O_4S+H\text{-}CO_2]^+$
		323	$[C_{16}H_{21}N_3O_6S+H\text{-}NH_3\text{-}CO_2]^+$
		295	$[C_{16}H_{21}N_3O_6S+H\text{-}NH_3\text{-}CO_2\text{-}CO]^+$
		189	$[C_{16}H_{21}N_3O_6S+H\text{-}NH_3\text{-}CO_2\text{-}CO\text{-}C_7H_6O]^+$
		160	$[C_6H_{10}NO_2S]^+$
9.5	$C_{15}H_{21}N_3O_4S$	340 [M + 1]	$[C_{15}H_{21}N_3O_4S+H]^+$
	(339 g/mol)	323	$[C_{15}H_{21}N_3O_4S+H\text{-}NH_3]^+$
	APlA[1]	295	$[C_{15}H_{21}N_3O_4S+H\text{-}NH_3\text{-}CO_2]^+$
		277	$[C_{15}H_{21}N_3O_4S+H\text{-}NH_3\text{-}CO_2\text{-}H_2O]^+$
		189	$[C_{15}H_{21}N_3O_4S+H\text{-}NH_3\text{-}CO\text{-}C_7H_6O]^+$
10.8	$C_{16}H_{21}N_3O_6S$	384 [M + 1]	$[C_{16}H_{21}N_3O_6S+H]^+$
	(383 g/mol)	367	$[C_{16}H_{21}N_3O_6S+H\text{-}NH_3]^+$
	APcA[2]	349	$[C_{16}H_{21}N_3O_6S+H\text{-}NH_3\text{-}H_2O]^+$
		340	$[C_{16}H_{21}N_3O_4S+H\text{-}CO_2]^+$
		323	$[C_{16}H_{21}N_3O_6S+H\text{-}NH_3\text{-}CO_2]^+$
		189	$[C_{16}H_{21}N_3O_6S+H\text{-}NH_3\text{-}CO_2\text{-}CO\text{-}C_7H_6O]^+$
		160	$[C_6H_{10}NO_2S]^+$
11.7	$C_{15}H_{21}N_3O_4S$	340 [M + 1]	$[C_{15}H_{21}N_3O_4S+H]^+$
	(339 g/mol)	323	$[C_{15}H_{21}N_3O_4S+H\text{-}NH_3]^+$
	APlA[2]	295	$[C_{15}H_{21}N_3O_4S+H\text{-}NH_3\text{-}CO_2]^+$
		277	$[C_{15}H_{21}N_3O_4S+H\text{-}NH_3\text{-}CO_2\text{-}H_2O]^+$
		189	$[C_{15}H_{21}N_3O_4S+H\text{-}CO\text{-}NH_3\text{-}C_7H_6O]^+$
13.4	$C_{10}H_8N_2O_2$	189	$[C_{10}H_8N_2O_2+H]^+$
	(188 g/mol)	171	$[C_{10}H_8N_2O_2+H\text{-}H_2O]^+$
	BhP	130	$[C_9H_8N]^+$

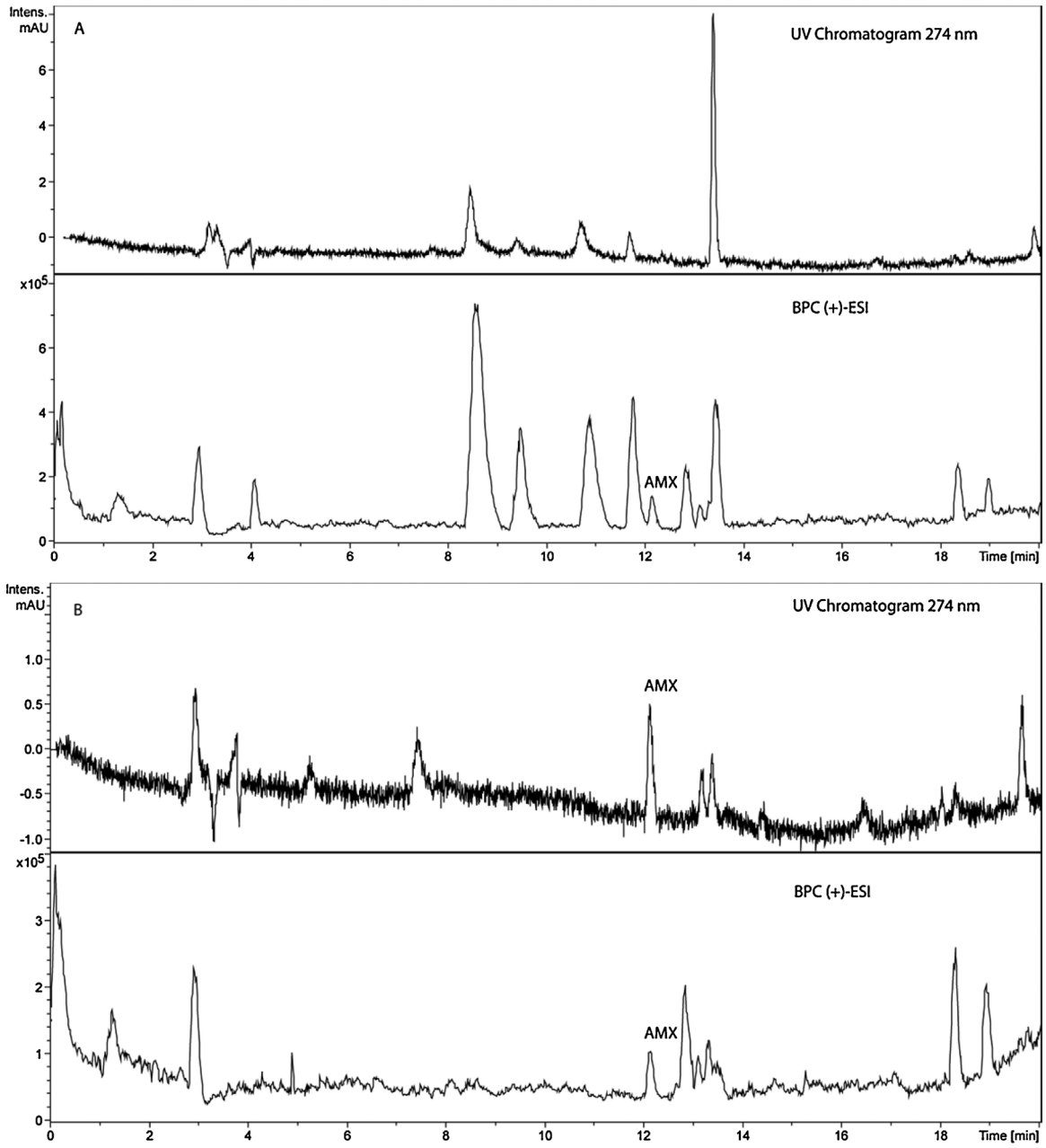

Fig. 10. UV (274 nm) and BPC (+)-ESI of TiO_2/zeolite photocatalysis of AMX. (A) After initial hydrolysis and (B) after 240 min of irradiation.

fragments of *m*/*z* 323. A compound with *m*/*z* 189 was assigned to phenol hydroxypyrazine (PHp) and this highly fluorescent degradant dominated the chromatogram upon UV-detection [63]. Additional degradation products were found, but their structures could not be determined without further isolation and characterization.

After irradiation for 4 h, almost all thermal degradants had been removed and only small amounts were still detectable by LC-MS (Fig. 10b). Various hydroxylated products have been reported by Klauson et al. from visible light photocatalysis with doped titania [44] and by Trovó et al. during solar photo-Fenton reactions [32]. In both cases, low intensity light was applied to allow for the detection

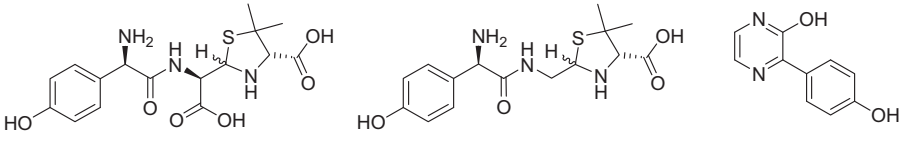

APcA
M_W = 383 g/mol

APlA
M_W = 339 g/mol

PHp
M_W = 188 g/mol

Fig. 11. Hydrolysis products (APcA and APlA as diastereoisomeric mixtures) of AMX confirmed by LC-MS analyses prior to irradiation under TiO_2/zeolite photocatalytic conditions.

and subsequent identification of degradants. The reaction mixtures obtained in this study were screened by LC-MS for the characteristic ions of the reported degradants, but their presence could not be confirmed without doubt. The extreme UV-light conditions used and the prolonged irradiation time applied likely caused rapid degradation of all primary and secondary decomposition products. The absence of any major peaks in the MS spectra suggests the formation of a variety of smaller degradants. The observed mineralization rate of 25% further confirmed that the degradation process was highly efficient under these conditions.

Samples taken from direct photolysis and TiO_2 P25 photocatalysis were also examined for their thermal stability. In both cases, AMX remained largely intact and only trace amounts of thermal degradants could be detected in the corresponding LC-MS spectra. At the end of the irradiations, AMX was still detectable but no specific degradation products could again be identified.

4. Conclusions

TiO_2/zeolite-photocatalysis presents a feasible methodology for the degradation of the antibiotic AMX. Of the various IPAs synthesized, the material from acid-alkaline pre-treatment and calcination at 300 °C showed the best performance attributed to its favourable surface structure and TiO_2 content. Overall, this IPA material possessed the highly desirable properties of the individual components: (1) the adsorption capability of zeolite, anchoring AMX on its surface near the photocatalyst, (2) the acidic nature of zeolite, effectively converting AMX, at least in part, by hydrolysis and (3) the photocatalytic activity of TiO_2, consecutively degrading AMX and its hydrolysis products. While the efficiency of the IPA decreased somewhat after repeated usage, its photoactivity may be restored by subsequent calcination as demonstrated by Sharma et al. for TiO_2/mordenite hybrid materials [61]. Together with the ease of catalyst recycling and the relative effectiveness of mineralization, this IPA material has a distinct advantage over traditionally applied TiO_2 in suspension [21]. This work also demonstrated the importance of pH for AMX removal as thermal hydrolysis can occur simultaneously with photodegradation. Further effort is required to better understand the contributions of thermal processes towards the overall degradation. Likewise, more research into the utilisation of TiO_2/zeolite IPAs for the treatment of other commonly present pharmaceutical pollutants and their metabolites is imperative. Ultimately, IPAs may offer novel treatment options for wastewater effluents from pharmaceutical plants [71].

Acknowledgements

This work was supported by research grants from James Cook University (FAIG award 2009 and GRS awards 2011 and 2012). D.K. also thanks the Malaysian Government for a University Doctorate Training Award. The authors also wish to thank Evonik industries for the donation of Titanium dioxide P25 Aeroxide®, Miss Saira Mumtaz (JCU) for technical assistance and Mr. Stephen Boyle (AIMS) for TOC analyses.

References

[1] O. Carp, C.L. Huisman, A. Reller, Prog. Solid State Chem. 32 (2004) 33–177.
[2] J.-M. Herrmann, Cat. Today 53 (1999) 115–129.
[3] M.N. Chong, B. Jin, C.W.K. Chow, C. Saint, Water Res. 44 (2010) 2997–3027.
[4] A.Y. Shan, T.I.M. Ghazi, S.A. Rashid, Appl. Cat. A: Gen. 389 (2010) 1–8.
[5] D. Keane, K. Nolan, A. Morrissey, M. Oelgemöller, S. Basha, J. Tobin, in: A.G. Griesbeck, M. Oelgemöller, F. Ghetti (Eds.), CRC Handbook of Organic Photochemistry and Photobiology, 3rd ed., CRC, Press, Boca Raton, 2012, pp. 935–962, Chapter 37.
[6] S. Basha, C. Barr, D. Keane, K. Nolan, A. Morrissey, M. Oelgemöller, J.M. Tobin, Photochem. Photobiol. Sci. 10 (2011) 1014–1022.
[7] S. Liu, M. Lim, R. Amal, Chem. Eng. Sci. 105 (2014) 46–52.
[8] F. Haque, E. Vaisman, C.H. Langford, A. Kantzas, J. Photochem. Photobiol. A: Chem. 169 (2005) 21–27.
[9] M.E. Fabiyi, R.L. Skelton, J. Photochem. Photobiol. A: Chem. 132 (2000) 121–128.
[10] J.Q. Albarelli, D.T. Santos, S. Murphy, M. Oelgemöller, Water Sci. Technol. 60 (2009) 1081–1087.
[11] S. Wang, Y. Peng, Chem. Eng. J. 156 (2010) 11–24.
[12] M. Huang, C. Xu, Z. Wu, Y. Huang, J. Lin, J. Wu, Dyes Pigments 77 (2008) 327–334.
[13] A. Ates, C. Hardacre, J. Colloid Interface Sci. 372 (2012) 130–140.
[14] E.G. Derouane, J.C. Védrine, R. Ramos Pinto, P.M. Borges, L. Costa, M.A.N.D.A. Lemos, R. Ramôa Riberto, Cat. Rev. Sci. Eng. 55 (2013) 454–515.
[15] Y. Lester, H. Mamane, D. Avisar, Water Air Soil Pollut. 223 (2012) 1639–1647.
[16] C.Y. Kuo, C.Y. Pai, C.C. He, C.J. Lin, C.M. Cheng, Water Sci. Technol. 65 (2012) 1963–1969.
[17] C. Wang, H. Shi, Y. Li, Appl. Surf. Sci. 257 (2011) 6873–6877.
[18] F. Li, Y. Jiang, L. Yu, Z. Yang, T. Hou, S. Sun, Appl. Surf. Sci. 252 (2005) 1410–1416.
[19] K. Kümmerer, Chemosphere 45 (2001) 957–969.
[20] K. Kümmerer, J. Environ. Manag. 90 (2009) 2354–2366.
[21] D. Kanakaraju, B.D. Glass, M. Oelgemöller, Environ. Chem. Lett. 12 (2014) 27–47.
[22] A.E. Bird, Anal. Profiles Drug Subst. Excip. 23 (1994) 1–52.
[23] R. Andreozzi, V. Caprio, C. Ciniglia, M. De Champdoré, R. Lo Giudice, R. Marotta, E. Zuccato, Environ. Sci. Technol. 38 (2004) 6832–6838.
[24] A.F. Martins, F. Mayer, E.C. Confortin, C.D. Frank, Clean 37 (2009) 365–371.
[25] H. Zia, N. Shalchian, F. Borhanian, Canad. J. Pharm. Sci. 12 (1977) 80–83.
[26] E. Nägele, R. Moritz, J. Am. Soc. Mass. Spectrom. 16 (2005) 1670–1676.
[27] E.K. Putra, R. Pranowo, J. Sunarso, N. Indraswati, S. Ismadji, Water Res. 43 (2009) 2419–2430.
[28] A.J. Watkinson, E.J. Murby, D.W. Kolpin, S.D. Costanzo, Sci. Total Environ. 407 (2009) 2711–2723.
[29] I. Michael, L. Rizzo, C.S. McArdell, C.M. Manaia, C. Merlin, T. Schwartz, C. Dagot, D. Fatta-Kassinos, Water Res. 47 (2013) 957–995.
[30] X. Li, T. Shen, D. Wang, X. Yue, X. Liu, Q. Yang, J. Cao, W. Zheng, G. Zeng, J. Environ. Sci. 24 (2012) 269–275.
[31] E. Deschamps, O. Vasconcelos, L. Lange, C.L. Donnici, M.C. daSilva, J.A. Sales, Braz. J. Pharmac. Sci. 48 (2012) 727–736.
[32] A.G. Trovó, R.F.P. Nogueira, A. Agüera, A.R. Fernandez-Alba, S. Malato, Water Res. 45 (2011) 1394–1402.
[33] E.S. Elmolla, M. Chaudhuri, Desalination 256 (2010) 43–47.
[34] E.S. Elmolla, M. Chaudhuri, J. Hazard. Mat. 170 (2009) 666–672.
[35] C. Mavronikola, M. Demetriou, E. Hapeshi, D. Partassides, C. Michael, D. Mantzavinos, D. Kassinos, J. Chem. Technol. Biotechnol. 84 (2009) 1211–1217.
[36] A.G. Trovó, S.A.S. Melo, R.F.P. Nogueira, J. Photochem. Photobiol. A: Chem. 198 (2008) 215–220.
[37] F. Javier Benitez, J.L. Acero, F.J. Real, G. Roldán, Chemosphere 77 (2009) 53–59.
[38] R. Andreozzi, M. Canterino, R. Marotta, N. Paxeus, J. Hazard. Mat. 122 (2005) 243–250.
[39] Y.J. Jung, W.G. Kim, Y. Yoon, J.-W. Kang, Y.M. Hong, H.W. Kim, Sci. Total Environ. 420 (2012) 160–167.
[40] J.H.O.S. Pereira, A.C. Reis, O.C. Nunes, M.T. Borges, V.J.P. Vilar, R.A.R. Boaventura, Environ. Sci. Pollution Res. (2013) 1–12.
[41] D. Dimitrakopoulou, I. Rethemiotaki, Z. Frontistis, N.P. Xekoukoulotakis, D. Venieri, D. Mantzavinos, J. Environ. Manag. 98 (2012) 168–174.
[42] J. Kockler, D. Kanakaraju, B.D. Glass, M. Oelgemöller, J. Sustain. Sci. Manag. 7 (2012) 23–29.
[43] E.S. Elmolla, M. Chaudhuri, Desalination 252 (2010) 46–52.
[44] D. Klauson, J. Babkina, K. Stepanova, M. Krichevskaya, S. Preis, Cat. Today 151 (2010) 39–45.
[45] E.S. Elmolla, M. Chaudhuri, J. Hazard. Mat. 173 (2010) 445–449.
[46] M.E. Trujillo, D. Hirales, M.E. Rincón, J.F. Hinojosa, G.L. Leyva, F.F. Castillón, J. Mat. Sci. 48 (2013) 6778–6785.
[47] O. Korkuna, R. Leboda, J. Skubiszewska-Zięba, T. Vrublevs'ka, V.M. Gun'ko, J. Ryczkowski, Microp. Mesop. Mat. 87 (2006) 243–254.
[48] M. Nikazar, K. Gholivand, K. Mahanpoor, Desalination 219 (2008) 293–300.
[49] B. Ohtani, Y. Ogawa, S.-i. Nishimoto, J. Phys. Chem. B 101 (1997) 3746–3752.
[50] T.A. Kandiel, L. Robben, A. Alkaim, D. Bahnemann, Photochem. Photobiol. Sci. 12 (2013) 602–609.
[51] M.N. Chong, V. Vimonses, S.M. Lei, B. Jin, C. Chow, C. Saint, Microp. Mesop. Mat. 117 (2009) 233–242.
[52] B. Zhu, L. Zou, J. Environ. Manag. 90 (2009) 3217–3225.
[53] S. Gomez, C.L. Marchena, L. Pizzio, L. Pierella, J. Hazard. Mat. 258–259 (2013) 19–26.
[54] A.T. Najafabadi, F. Taghipour, J. Photochem. Photobiol. A: Chem. 248 (2012) 1–7.
[55] Y. Xu, C.H. Langford, J. Phys. Chem. B 101 (1997) 3115–3121.
[56] Y. Xu, C.H. Langford, J. Phys. Chem. 99 (1995) 11501–11507.
[57] A.G. Thomas, K.L. Syres, Chem. Soc. Rev. 41 (2012) 4207–4217.
[58] F. Li, S. Sun, Y. Jiang, M. Xia, M. Sun, B. Xue, J. Hazard. Mat. 152 (2008) 1037–1044.
[59] W. Zhang, L.D. Zou, L.Z. Wang, Appl. Cat. A: Gen. 371 (2009) 1–9.
[60] Z. Shi, S. Yao, C. Sui, Cat. Sci. Technol. 1 (2011) 817–822.
[61] M.V.P. Sharma, V. Durgakumari, M. Subrahmanyam, J. Hazard. Mat. 160 (2008) 568–575.
[62] B. Ohtani, O.O. Prieto-Mahaney, D. Li, R. Abe, J. Photochem. Photobiol. A: Chem. 216 (2010) 179–182.
[63] I. Gozlan, A. Rotstein, D. Avisar, Chemosphere 91 (2013) 985–992.
[64] A.I. Doadrio, J. Sotelo, An. Real. Acad. Farm. 55 (1988) 203–212.
[65] U.I. Gaya, A.H. Abdullah, J. Photochem. Photobiol. C: Photochem. Rev. 9 (2008) 1–12.

[66] A. Pérez-Parada, A. Agüera, M.D. Gómez-Ramos, J.F. García-Reyes, H. Heinzen, A.R. Fernández-Alba, Rapid Comm. Mass Spectrom. 25 (2011) 731–742.
[67] I. Gozlan, A. Rotstein, D. Avisar, Environ. Chem. 7 (2010) 435–442.
[68] L. Valvo, E. Ciranni, R. Alimenti, S. Alimonti, R. Draisci, L. Giannetti, L. Lucentini, J. Chromat. A 797 (1998) 311–316.
[69] Z. Yongxin, E. Roets, R. Busson, G. Janssen, J. Hoogmartens, Bull. Soc. Chim. Belg. 106 (1997) 67–71.
[70] E. Roets, P. de Pourcq, S. Toppet, J. Hoogmartens, H. Vanderhaeghe, D.H. Williams, R.S. Smith, J. Chromat. 303 (1984) 117–129.
[71] A.M. Deegan, B. Shaik, K. Nolan, K. Urell, M. Oelgemöller, J. Tobin, A. Morrissey, Int. J. Environ. Sci. Technol. 8 (2011) 649–666.